

Free coherent evolution of a coupled atomic spin system initialized by electron scattering

Veldman, Lukas M.; Farinacci, Laëtitia; Rejali, Rasa; Broekhoven, Rik; Gobeil, Jérémie; Coffey, David; Ternes, Markus; Otte, Alexander F.

DOI

[10.1126/science.abg8223](https://doi.org/10.1126/science.abg8223)

Publication date

2021

Document Version

Accepted author manuscript

Published in

Science

Citation (APA)

Veldman, L. M., Farinacci, L., Rejali, R., Broekhoven, R., Gobeil, J., Coffey, D., Ternes, M., & Otte, A. F. (2021). Free coherent evolution of a coupled atomic spin system initialized by electron scattering. *Science*, 372(6545), 964-968. Article abg8223. <https://doi.org/10.1126/science.abg8223>

Important note

To cite this publication, please use the final published version (if applicable).
Please check the document version above.

Copyright

Other than for strictly personal use, it is not permitted to download, forward or distribute the text or part of it, without the consent of the author(s) and/or copyright holder(s), unless the work is under an open content license such as Creative Commons.

Takedown policy

Please contact us and provide details if you believe this document breaches copyrights.
We will remove access to the work immediately and investigate your claim.

Free coherent evolution of a coupled atomic spin system initialized by electron scattering

Authors: Lukas M. Veldman¹, Laëtizia Farinacci¹, Rasa Rejali¹, Rik Broekhoven¹, Jérémie Gobeil¹, David Coffey¹, Markus Ternes^{2,3}, Alexander F. Otte^{1*}.

Affiliations:

¹ Department of Quantum Nanoscience, Kavli Institute of Nanoscience, Delft University of Technology, Lorentzweg 1, 2628 CJ Delft, The Netherlands

² RWTH Aachen University, Institute of Physics, D-52074 Aachen, Germany

³ Peter-Grünberg-Institute, Forschungszentrum Jülich, D-52425 Jülich, Germany

*Correspondence to: a.f.otte@tudelft.nl

Abstract:

Full insight into the dynamics of a coupled quantum system depends on the ability to follow the effect of a local excitation in real-time. Here, we trace the free coherent evolution of a pair of coupled atomic spins by means of scanning tunneling microscopy. Rather than using microwave pulses, we employ a direct-current pump-probe scheme to detect the local magnetization following a current-induced excitation performed on one of the spins. Making use of magnetic interaction with the probe tip, we are able to tune the relative precession of the spins. We show that only if their Larmor frequencies match, the two spins can entangle, causing angular momentum to be swapped back and forth. These results provide insight into the locality of electron-spin scattering, and set the stage for controlled migration of a quantum state through an extended spin lattice.

One Sentence Summary:

Using STM-based electron spin resonance and DC pump-probe spectroscopy we track the free spin evolution of two entangled atoms.

Main Text:

One of the longstanding goals in experimental physics is the ability to create a *quantum simulator*: an engineered system of coupled quantum degrees of freedom that can be initialized in an arbitrary state, allowing one to observe its intrinsic free evolution (1). In principle, scanning tunneling microscopy (STM) offers each of these ingredients. Individual magnetic atoms can be spatially arranged and studied by means of spin-polarized tunneling (2,3) and electron tunneling spectroscopy (4,5), allowing to respectively probe their local magnetization state and energy

configuration. However, due to their slow timescales, these techniques have been able to observe the dynamic spin processes only indirectly (6-8).

In recent years, the STM toolbox was expanded to include pump-probe spectroscopy – allowing spin relaxation to be probed on the nanosecond timescale (9,10) – as well as electron spin resonance performed locally at the probe tip (ESR-STM) (11). ESR-STM, combined with microwave AC pulsing schemes, enabled the observation of the coherent time evolution of a single atomic spin (12), on par with achievements in semiconductor spin qubits (13,14) and NV centers (15). However, in order to demonstrate free evolution of a pair of entangled spins, the initial excitation has to be sufficiently fast to compete with the intrinsic dynamics set by the coupling strength. ESR-STM uses a Rabi flop process for initialization, the rate of which is limited by the radio-frequency (RF) power available at the probe tip.

Here, by sequentially combining ESR-STM and DC pump-probe techniques, we demonstrate the detection of free, coherent flip-flop evolution of two coupled spin-1/2 atoms resulting from an electron-induced spin excitation that is nearly instantaneous compared to the typical duration of a Rabi rotation. Using the energy resolution of ESR-STM we tune the eigenstates of two coupled spin-1/2 particles from Zeeman states $|\uparrow\uparrow\rangle, |\downarrow\uparrow\rangle, |\uparrow\downarrow\rangle, |\downarrow\downarrow\rangle$ to singlet-triplet states $|\uparrow\uparrow\rangle, |-\rangle, |+\rangle, |\downarrow\downarrow\rangle$ by varying the tip height (11,16,17). Subsequently, using a DC pump-probe scheme, we excite and read out the spin projection of one of the two spins with nanosecond resolution. This is in contrast to previous efforts, where microwave AC pulses were used to control and readout spins (12). Rather than by means of a Rabi rotation, here the coherent evolution is initiated directly through an electron-spin scattering event.

As we increase the delay between pump and probe pulses, we observe an oscillating magnetization for the spin underneath the tip which we attribute to a flip-flop interaction between the two spins (18,19). This implies that the excitation process due to tunneling electron scattering is local: it only consists of a spin-flip on the atom underneath the tip, irrespective of the energy eigenstates of the system. This is a noteworthy result in the light of previous works, where it was deemed sufficient to consider electron-induced spin excitations as transitions between energy eigenstates (20-22).

We use a low-temperature STM to manipulate individual hydrogenated Ti atoms, henceforth referred to as TiH, on top of bilayer MgO islands on a Ag(100) crystal. To obtain spin polarization, we deposit Fe atoms and transfer them to the tip apex (23). The ESR and pump-probe experiments are performed by applying the RF voltage and pulse trains to the tip, at temperatures of 1.5 K and 400 mK, respectively. We use an external field $B_{\text{ext}} = 450$ mT in-plane at 14° angle with respect to the MgO lattice to separate the energy levels via Zeeman splitting.

We study TiH species without any observable nuclear spin adsorbed on bridge sites with different orientations with respect to the external magnetic field, as sketched in Fig. 1A. TiH on MgO has been shown to be an effective spin-1/2 particle with an anisotropic g-factor (24,25). In agreement with these studies, we observe different ESR resonance frequencies for the two species: for the

spin S_v vertically oriented TiH species (blue) we find a g-factor $g_v = 1.75$ while for the spin S_h of the horizontal TiH (green) we find $g_h = 1.95$ (supplementary sections S1 and S2).

Figures 1B and C demonstrate how we use the effective magnetic field emanating from the tip on one of the two atoms to tune the level of entanglement between the spins (10, 17). If the two spins experience the same effective Zeeman splitting, they precess at identical Larmor frequencies resulting in entangled states. Since we want to reach entanglement at a finite tip field, the two spins need to be inherently detuned in absence of the tip. For this reason, we build heterodimers out of vertically and horizontally oriented TiH species (Fig. 1B, see supplementary section S3 for details).

The dimers are engineered to have a spacing of 1.3 nm, corresponding to a coupling strength in the order of tens of MHz. This coupling strength is chosen to ensure that the dynamics of the local magnetization are slow enough to be probed by our experimental setup, which is limited to ~ 5 ns pulses, but still faster than the ~ 100 ns decoherence time of TiH dimers (17). At this distance, the atoms interact both via exchange and dipolar interactions. The Hamiltonian of the system can be written as (supplementary section S4):

$$H = (J + 2D)S_v^z S_h^z + (J - D)(S_v^x S_h^x + S_v^y S_h^y) - \mu_B B_{\text{ext}}(g_v S_v^z + g_h S_h^z) - \mu_B B_{\text{tip}} g_v S_v^z$$

where J and D are the exchange and dipolar coupling parameters, respectively. The two last terms account for the Zeeman splitting due to the external (B_{ext}) and effective tip (B_{tip}) fields, which, based on their relative strengths, we assume to be aligned. In supplementary section S6, we discuss the justification and limits of this assumption.

We separate the exchange and dipolar contributions by performing the experiment on two heterodimers as sketched in Figs. 2A (dimer A) and B (dimer B). The two dimers are equidistant, yielding identical exchange couplings. However, as they are oriented at different angles with respect to the external field, their dipolar coupling strengths differ. This is confirmed by ESR measurements performed on top of the vertically oriented TiH of each dimer with the tip well away from the tuning point (Figs. 2A and B). In this situation, the $S_x S_x$ and $S_y S_y$ components of the coupling (Eq. 1) average out over time as the spins precess with different Larmor frequencies. The resulting coupling, being mediated through the $S_z S_z$ terms only, is effectively Ising-like. Due to the composition of the eigenstates and because ESR can only flip the spin underneath the tip (26), only transitions I and II are observed (see Fig. 1C). The measured splitting between these two ESR resonances corresponds to $J + 2D$, and thus, is different for the two heterodimers (see Figs. 2A and B).

In order to probe the full energy level diagram of Fig. 1C and identify the exact tuning point for maximal entanglement, we perform ESR measurements at various tip heights for each dimer (Figs. 2C and 2D). We observe two sets of peaks that, upon tip approach, shift together and broaden due to decoherence effects (27). These two sets of resonances can be assigned to

transitions I & II and III & IV in Fig. 1C. Away from the tuning point, only one of these pairs is observed: transition I & II before the tuning point and transition III & IV after it. As the energy eigenstates become more entangled near the tuning point, all four transitions become accessible. Due to the opposite signs of the dipolar coupling contributions, the two dimers show slightly different behaviors: transitions II and III intersect twice for dimer A while they stay apart for dimer B. We find $J = 67 \pm 2$ MHz, $D = 2 \pm 1$ MHz for dimer A and $D = -15 \pm 1$ MHz for dimer B (supplementary section S5).

We now arrive at the second stage of the experiment where we measure the free time evolution of the spins. We use a pump probe scheme to excite and measure the spin state of the atom underneath the tip for various degrees of entanglement. When the tip height is far away from the tuning point, the pump probe experiments show the onset of an exponential decay similar to the decay signal of a single excited spin (Figs. 2E and F, top and bottom curves) (9). By contrast, when tuned, we observe a clear oscillation with a frequency of 64 ± 1 MHz for dimer A and 84 ± 1 MHz for dimer B. We attribute these oscillations to the flip-flop interaction of strength $J - D$ between the two atoms in the dimer.

The dynamics of the flip-flop interaction can be well understood by describing the time evolution of the combined density matrix of the two spins within a dissipative Bloch-Redfield framework (28,29), which accounts for the uncorrelated electron baths in sample and tip (Fig. 3A, see supplementary section S7 for details). In Figs. 3B-E we show density matrices in the energy basis obtained by numerical simulation for a perfectly tuned dimer at different moments in time after the pump pulse.

During the pump pulse, the system is pushed into a coherent superposition of its excited states (Fig. 3B). These add up to a net $|\downarrow\uparrow\rangle$ magnetization (where the left arrow corresponds to the spin underneath the tip), as a result of spin pumping (23). This net magnetization is reflected in the off-diagonal terms, which correspond to the coherence between the $|-\rangle$ and $|+\rangle$ states. Due to the finite thermal occupation of the excited states in the initial Boltzmann distribution, the pump pulse also populates the higher energy $|\downarrow\downarrow\rangle$ state. Immediately after the pulse, the off-diagonals begin to oscillate between positive and negative values (Figs. 3C,D), giving rise to the observed periodicity in the magnetization (see inset of panel a). Due to interaction with the electron baths, the oscillations decay over an effective decoherence time and eventually the populations evolve back towards thermal equilibrium (Fig. 3E). We estimate the decoherence time to be 60 ns and 130 ns for the relaxation time (supplementary section S8).

We now proceed to the effect of detuning on the flip-flop oscillations. For this purpose, we perform pump-probe experiments at different current setpoints around the tuning point: ~ 28 pA for dimer A and ~ 40 pA for dimer B (Figs. 4A and B). As expected, the oscillations diminish rapidly as we tune away from these values. Depending on the microscopic tip apex, we observe a small difference in tuning height between ESR (Fig. 2) and pump probe measurements (Fig. 4). We attribute this discrepancy to the temperature dependence of the spin polarized current as the two different experiments were carried out at different temperatures (supplementary section S9).

To gain insight into the effect of detuning on the spin dynamics, we map the effective two-level system of the inner 2×2 matrix of the density matrix onto a Bloch sphere. For clarity, the axes of the sphere are fixed to be the energy eigenstates of the fully tuned case, while the projected spin state evolution is plotted for different levels of detuning (Fig 4C-F). As can be seen from the density matrices in Fig. 3, the spin state always has components outside the inner 2×2 matrix, meaning that the projection in Fig. 4 never reaches the surface of the sphere.

When the dimer is in tune (Fig. 4C), the state moves fully within the vertical plane of the Bloch sphere, making maximal flip-flops between $|\uparrow\downarrow\rangle$ and $|\downarrow\uparrow\rangle$. With increasing detuning, the axis around which the state rotates moves as the eigenstates of the system gradually tilts towards the vertical. The difference between the projected maxima and minima of the oscillation onto the vertical axis gets smaller and thus the oscillation amplitude decreases, consistent with our experimental observations.

The observed flip-flop frequency remains constant as a function of detuning. This is surprising, as the energy splitting is supposed to increase away from the tuning point, causing an increase in the frequency (see supplementary section S10). Since the in-plane anisotropy of the g-factor indicates a partially unquenched orbital moment resulting from the crystal-field symmetry of the bridge sites, as previously observed for the out-of-plane direction on TiH species on oxygen binding sites (24), the observed discrepancy may be related to this orbital moment.

In conclusion, by combining the energy resolution of ESR-STM and the time resolution of DC pump-probe spectroscopy, we have demonstrated a new experimental procedure enabling the observation of the free coherent evolution of coupled atomic spins. As the dynamic processes are initialized by means of a coherence-preserving pulse in the tunneling current, our method provides new insight into the physics of electron-spin scattering that could not be obtained by pulsed ESR-STM methods (12). Specifically, we find that only the spin directly underneath the tip is affected by the spin excitation, irrespective of the global quantum state. In conjunction with the recent demonstration of pulsed ESR-STM, our technique offers pathways towards coherent manipulation of extended atomic spin arrays. The ability to perform a very local, nearly instantaneous, coherent spin flip inside an extended spin lattice constitutes an essential building block for advances in spintronic engineering as well as studies into the propagation of spin waves.

References and Notes:

1. J. I. Cirac, P. Zoller, Goals and opportunities in quantum simulation. *Nat. Phys.* **8**, 264-266 (2012).
2. S. Heinze, M. Bode, A. Kubetzka, O. Pietzsch, X. Nie, S. Blügel, R. Wiesendanger, Real-space imaging of two-dimensional antiferromagnetism on the atomic scale. *Science* **288**, 1805-1808 (2000).
3. F. Meier, L. Zhou, J. Wiebe, R. Wiesendanger, Revealing magnetic interactions from single-atom magnetization curves. *Science* **320**, 82-86 (2008).

4. A. J. Heinrich, J. Gupta, C. Lutz, D. Eigler, Single-atom spin-flip spectroscopy. *Science* **306**, 466-469 (2004).
5. C. F. Hirjibehedin, C. P. Lutz, A. J. Heinrich, Spin coupling in engineered atomic structures. *Science* **312**, 1021-1024 (2006).
6. M. Ternes, Spin excitations and correlations in scanning tunneling spectroscopy. *New. J. Phys.* **17**, 063016 (2015).
7. R. J. G. Elbertse, D. Coffey, J. Gobeil, A. F. Otte, Remote detection and recording of atomic-scale spin dynamics. *Comm. Phys.* **3**, 94 (2020).
8. L. Malavolti, G. McMurtrie, S. Rolf-Pissarczyk, S. Yan, J. A. J. Burgess, S. Loth, Minimally invasive spin sensing with scanning tunneling microscopy. *Nanoscale* **12**, 11619-11626 (2020).
9. S. Loth, M. Etzkorn, C. P. Lutz, D. M. Eigler, A. J. Heinrich, Measurement of Fast Electron Spin Relaxation Times with Atomic Resolution. *Science* **329**, 1628-1630 (2010).
10. S. Yan, D.-J. Choi, J. A. J. Burgess, S. Rolf-Pissarczyk, Sebastian Loth, Control of quantum magnets by atomic exchange bias. *Nature Nanotech.* **10**, 40-45 (2015).
11. S. Baumann, W. Paul, T. Choi, C. P. Lutz, A. Ardavan, A. J. Heinrich, Electron paramagnetic resonance of individual atoms on a surface. *Science* **350**, 417-420 (2015).
12. K. Yang, W. Paul, S.-H. Phark, P. Willke, Y. Bae, T. Choi, T. Esat, A. Ardavan, A. J. Heinrich, C. P. Lutz, Coherent spin manipulation of individual atoms on a surface. *Science* **366**, 509-512 (2019).
13. J. J. Pla, K. Y. Tan, J. P. Dehollain, W. H. Lim, J. J. L. Morton, D. N. Jamieson, A. S. Dzurak, A. Morello, A single-atom electron spin qubit in silicon. *Nature*, **489**, 541-545 (2012).
14. E. Kawakami, P. Scarlino, D. R. Ward, F. R. Braakman, D. E. Savage, M. G. Lagally, M. Friesen, S. N. Coppersmith, M. A. Eriksson, L. M. K. Vandersypen, Electrical control of a long-lived spin qubit in a Si/SiGe quantum dot. *Nature Nanotechnology* **9**, 666-670 (2014).
15. R. Hanson, V. V. Dobrovitski, A. E. Feiguin, O. Gywat, D. D. Awschalom, Coherent dynamics of a single spin interacting with an adjustable spin bath. *Science* **320**, 352-355 (2008).
16. K. Yang, Y. Bae, W. Paul, F. D. Natterer, P. Willke, J. L. Lado, A. Ferrón, T. Choi, J. Fernández-Rossier, A. J. Heinrich, C. P. Lutz, Engineering the Eigenstates of Coupled Spin-1/2 Atoms on a Surface. *Phys. Rev. Lett.* **119**, 227206 (2017).
17. Y. Bae, K. Yang, P. Willke, T. Choi, A. J. Heinrich, C. P. Lutz, Enhanced quantum coherence in exchange coupled spins via singlet-triplet transitions. *Sci. Adv.* **4**, eaau4159 (2018).
18. J. R. Petta, A. C. Johnson, J. M. Taylor, E. A. Laird, A. Yacoby, M. D. Lukin, C. M. Marcus, M. P. Hanson, A. C. Gossard, Coherent Manipulation of Coupled Electron Spins in Semiconductor Quantum Dots. *Science* **309**, 2180-2184 (2005).
19. Y. He, S. K. Gorman, D. Keith, J. G. Kreizer, M. Y. Simmons, A two-qubit gate between phosphorus donor electrons in silicon. *Nature* **571**, 371-375 (2019).
20. C. F. Hirjibehedin, C. Lin, A. F. Otte, M. Ternes, C. P. Lutz, B. A. Jones, A. J. Heinrich, Large Magnetic Anisotropy of a Single Atomic Spin Embedded in a Surface Molecular Network. *Science* **317**, 1199-1203 (2007).
21. A. F. Otte, M. Ternes, S. Loth, C. P. Lutz, C. F. Hirjibehedin, A. J. Heinrich, Spin excitations of a Kondo-screened atom coupled to a second magnetic atom, *Physical Review Letters* **103**, 107203 (2009).
22. A. Spinelli, B. Bryant, F. Delgado, J. Fernández-Rossier, A. F. Otte, Imaging of spin waves in atomically designed nanomagnets. *Nature materials* **13**, 782-785 (2014).
23. S. Loth, K. von Bergmann, M. Ternes, A. F. Otte, C. P. Lutz, A. J. Heinrich, Controlling the state of quantum spins with electric currents. *Nat. Phys.* **6**, 340-344 (2010).

24. M. Steinbrecher, W. M. J. van Weerdenburg, E. F. Walraven, N. P. E. van Mullekom, J. W. Gerritsen, F. D. Natterer, D. I. Badrtdinov, A. N. Rudenko, V. V. Mazurenko, M. I. Katsnelson, A. van der Avoird, G. C. Groenenboom, A. A. Khajetoorians, Quantifying the interplay between fine structure and geometry of an individual molecule on a surface. arxiv:2007.01928 (2020).
25. P. Willke, Y. Bae, K. Yang, Jose L. Lado, A. Ferrón, T. Choi, A. Ardavan, J. Fernández-Rossier, A. J. Heinrich, C. P. Lutz, Hyperfine interaction of individual atoms on a surface. *Science* **362**, 336-339 (2018).
26. T. Choi, W. Paul, S. Rolf-Pissarczyk, A. J. Macdonald, F. D. Natterer, K. Yang, P. Willke, C. P. Lutz, A. J. Heinrich, Atomic-scale sensing of the magnetic dipolar field from single atoms. *Nature nanotechnology*, **12**, 420-424 (2017).
27. P. Willke, W. Paul, F. D. Natterer, K. Yang, Y. Bae, T. Choi, J. Fernández-Rossier, A. J. Heinrich, C. P. Lutz, Probing quantum coherence in single-atom electron spin resonance. *Sci. Adv.* **4**, eaaq1543 (2018).
28. C. Cohen-Tannoudji, J. Dupont-Roc, G Grynberg, *Atom-Photon Interaction*. (Wiley and Sons Inc., New York, 1989).
29. F. Delgado, J. Fernández-Rossier, Spin decoherence of magnetic atoms on surfaces. *Progress in Surface Science* **92**, 40-82 (2017).
30. T. S. Seifert, S. Kovarik, D. M. Juraschek, N. A. Spaldin, P. Gambardella, S. Stepanow, Longitudinal and transverse electron paramagnetic resonance in a scanning tunneling microscope. *Sci. Adv.* **6**, 40 (2020).
31. S. Baumann, F. Donati, S. Stepanow, S. Rusponi, W. Paul, S. Gangopadhyay, I. G. Rau, G. E. Pacchioni, L. Gragnaniello, M. Pivetta, J. Dreiser, C. Piamonteze, C. P. Lutz, R. M. Macfarlane, B. A. Jones, P. Gambardella, A. J. Heinrich, H. Brune. Origin of Perpendicular Magnetic Anisotropy and Large Orbital Moment in Fe Atoms on MgO, *Phys. Rev. Lett.* **115**, 237202 (2015).
32. P. Willke, K. Yang, Y. Bae, A. J. Heinrich, C. P. Lutz, Magnetic resonance imaging of single atoms on a surface. *Nat. Phys.* **15**, 1005-1010 (2019).
33. C. P. Slichter, *Principles of Magnetic Resonance*. (Springer-Verlag, Berlin, 1990).
34. F. Delgado, J. Fernandez-Rossier, RKKY oscillations in the spin relaxation rates of atomic-scale nanomagnets. *Phys. Rev. B* **95**, 075413 (2017).
35. S. Loth, C. P. Lutz, A. J. Heinrich, Spin-polarized spin excitation spectroscopy. *New. J. Phys.* **12**, 125021 (2010).

Acknowledgments: We thank V. Kornich and L.M.K. Vandersypen for scientific discussions; **Funding:** The authors acknowledge support from the Netherlands Organisation for Scientific Research (NWO Vici Grant VI.C.182.016) and from the European Research Council (ERC Starting Grant 676895 “SPINCAD”). M.T. acknowledges support by the Heisenberg Program (grant no. TE 833/2-1) of the German Research Foundation; **Author contributions:** L.M.V., L.F. and R.R. performed the experiments. L.M.V., L.F., R.R., D.C. and J.G. implemented and optimized the experimental techniques. L.M.V and L.F. analyzed the experimental data. R.B. and M.T. developed the dissipative Bloch-Redfield model and performed the simulations. L.M.V., R.B. and A.F.O. designed the experiment. L.M.V., L.F., R.B., M.T. and A.F.O. wrote the manuscript, with input from all authors; **Competing interests:** The authors declare no competing interests; **Data and materials availability:** All data presented in this paper is publicly available via digital object identifier (DOI) 10.5281/zenodo.4467820.

List of Supplementary Materials:

Materials and Methods

Figures S1-S10

Table S1

References (30-35)

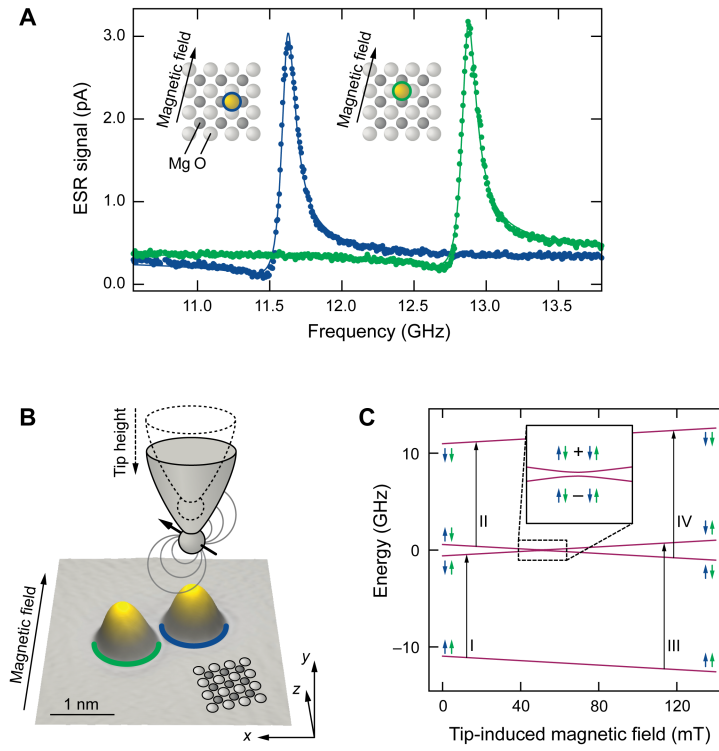


Fig. 1. Tuning the eigenstates of a TiH dimer using tip-induced magnetic field. (A) ESR measurements of single TiH adsorbed onto a vertical (blue) and a horizontal (green) bridge site ($T = 1.5$ K, $V_{\text{RF}} = 30$ mV, $I = 50$ pA, $V_{\text{DC}} = 60$ mV, $B_{\text{ext}} = 450$ mT). (B) STM topography of a TiH dimer with MgO lattice indication and schematic demonstrating tuning of the tip field. (C) Calculated energies and eigenstate compositions as function of tip field. An avoided crossing occurs at the point where the tip field compensates the g-factor difference. Roman numerals indicate the four possible ESR transitions.

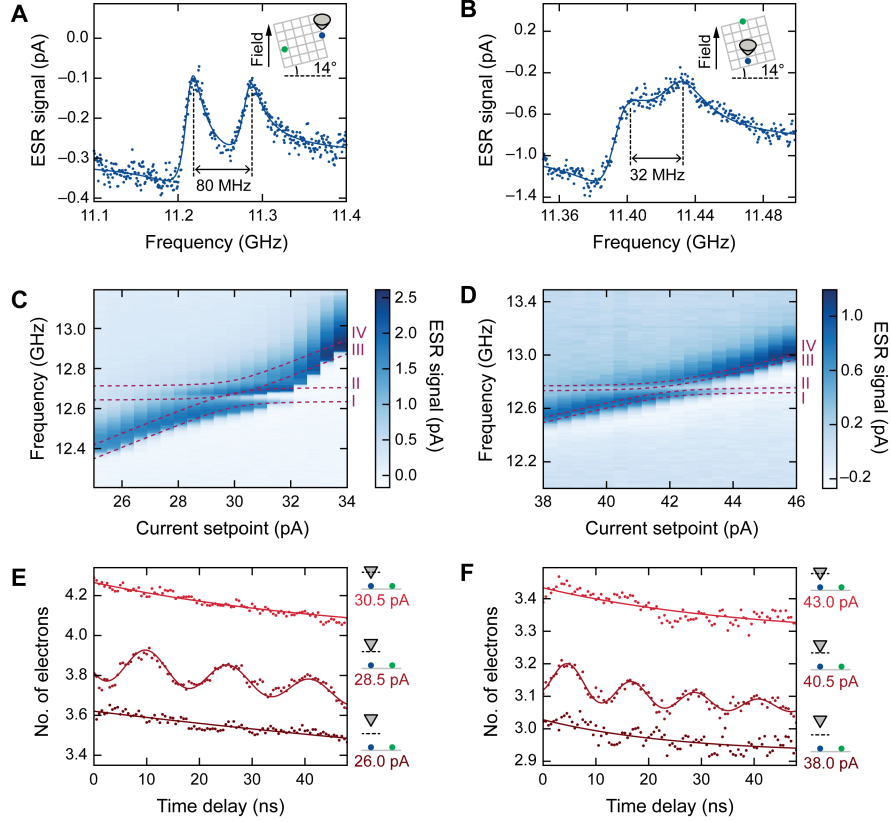


Fig. 2. Measurement of free coherent evolution at the tuning point. (A) and (B) ESR measurements on dimer A and dimer B ($T = 1.5$ K, $V_{RF} = 50$ mV, $I = 10$ pA, $V_{DC} = 60$ mV). Insets: schematic drawings of the dimer placement on the MgO lattice. (C) and (D) ESR measurements at various tip heights, showing an avoided crossing at the tuning point ($T = 1.5$ K, $V_{RF} = 50$ mV, $V_{DC} = 60$ mV). Dashed lines: guides to the eye marking ESR transitions. (E) Pump-probe measurements on dimer A, above, below and at the tuning point ($T = 400$ mK, setpoint voltage 60 mV, pulse width 7 ns). (F), same for dimer B (pulse width 5 ns). All pump-probe experiments use +100 mV pump and -100 mV probe pulses.

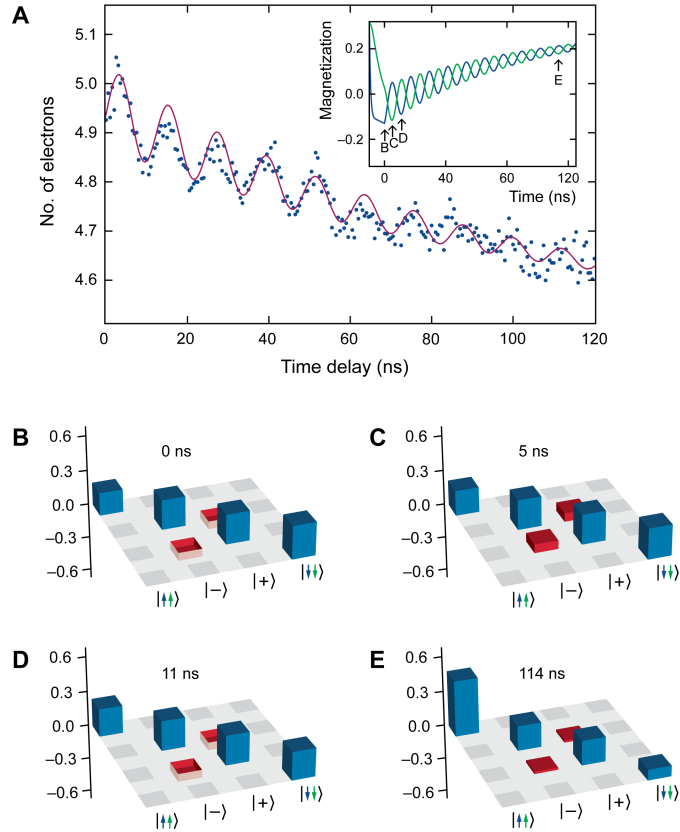


Fig. 3. Decoherence of the flip-flop oscillation. (A) Pump-probe measurement on dimer B showing the decay in amplitude of the oscillations ($T = 400$ mK, setpoint 40.5 pA, 60 mV, pulse width 7 ns). Solid line: calculated pump-probe signal. Inset: calculated magnetizations $\langle S_v^z \rangle$ (blue) and $\langle S_h^z \rangle$ (green); the origin of the time axis is set to coincide with the end of the pump pulse. (B-E) Density matrices at different times after the pump pulse (see inset of panel A). Off-diagonal elements are marked red for clarity.

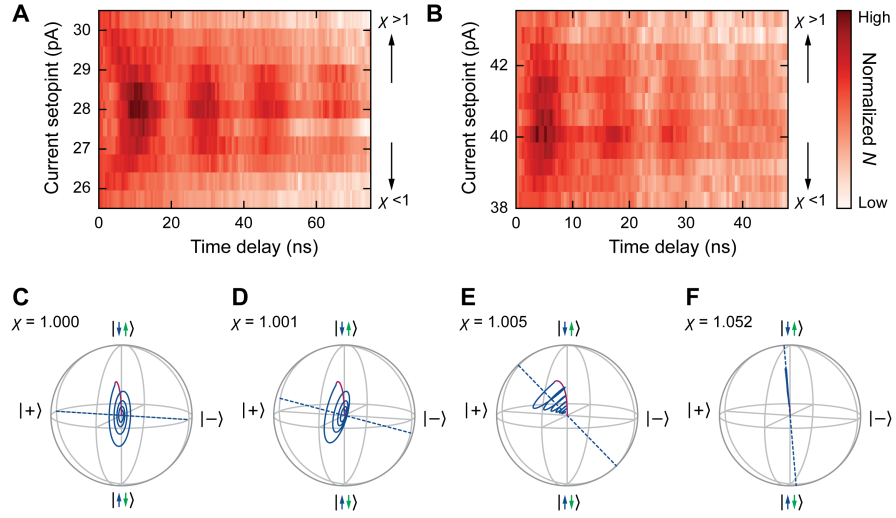


Fig. 4. Flip-flop oscillations as function of detuning. (A) and (B) Pump-probe measurements on dimer A and B at various tip heights (parameters same as in Fig. 2). (C-F) Bloch sphere representations of the state evolution at increasing levels of detuning, as indicated by the ratio $\chi = g_v(B_{\text{ext}} + B_{\text{tip}}) / g_h B_{\text{ext}}$. The Bloch spheres show the reduced state space between the $|\uparrow\downarrow\rangle$ and $|\downarrow\uparrow\rangle$ states. The excitation process due to the pump pulse is plotted in red, while the subsequent free evolution of the spin state is plotted in blue. For $\chi < 1$ the rotation axis (dashed blue line) tilts in the opposite direction.